Form Approved
OMB No. 0704-0188

1. AGENCY USE ONLY (Leave blank)	2. REPORT DATE	3. REPORT TYPE AND DATES COVERED
	Feb. 28, 1992	

4. TITLE AND SUBTITLE
Time and Space Resolved Electron Impact Excitation Rates in an rf Glow Discharge

5. FUNDING NUMBERS

6. AUTHOR(S)
Daniel E. Murnick & Yuan Li

7. PERFORMING ORGANIZATION NAME(S) AND ADDRESS(ES)
Department of Physics
Rutgers University
Newark, New Jersey 07102

8. PERFORMING ORGANIZATION REPORT NUMBER

9. SPONSORING/MONITORING AGENCY NAME(S) AND ADDRESS(ES)
U. S. Army Research Office
P. O. Box 12211
Research Triangle Park, NC 27709-2211

10. SPONSORING/MONITORING AGENCY REPORT NUMBER

11. SUPPLEMENTARY NOTES
The view, opinions and/or findings contained in this report are those of the author(s) and should not be construed as an official Department of the Army position, policy, or decision, unless so designated by other documentation.

12a. DISTRIBUTION/AVAILABILITY STATEMENT
Approved for public release; distribution unlimited.

12b. DISTRIBUTION CODE

13. ABSTRACT *(Maximum 200 words)*

Research on rf glow discharge plasmas was carried out to better understand the fundamental physics and chemistry of important aspects of plasma deposition and etching. A standard reference system for rf plasma processing research was utilized. Power, voltage and current waveforms were monitored and time and space resolved measurements were made using plasma induced emission (PIE). Nanosecond time resolution for PIE greatly expanded the utility of these plasma diagnostics over previous studies. Measurements were carried out with a prototype rf model discharge, atomic argon, concentrating on the important 4*s* levels 11.5eV above the ground state and the manifold of *p* levels coupled to these states by strong dipole transitions. Extensive analysis and computer modeling was carried out to reproduce the experimental data obtained and to test assumptions often used for this model system. Models of electron excitation "waves" were stringently tested and evaluated. The research concentrated on studying details of excitation waveforms as a function of pressure and rf power. Information on electron energy distribution functions were derived from the experimental results. New experimental techniques to enhance time and space resolution were developed.

14. SUBJECT TERMS	15. NUMBER OF PAGES
Glow Discharge Physics, Plasma Induced Emission, Plasma Processing	28
	16. PRICE CODE

17. SECURITY CLASSIFICATION OF REPORT	18. SECURITY CLASSIFICATION OF THIS PAGE	19. SECURITY CLASSIFICATION OF ABSTRACT	20. LIMITATION OF ABSTRACT
UNCLASSIFIED	UNCLASSIFIED	UNCLASSIFIED	UL

TIME AND SPACE RESOLVED ELECTRON IMPACT EXCITATION RATES IN AN RF GLOW DISCHARGE

FINAL REPORT

DANIEL E. MURNICK
AND
YUAN LI

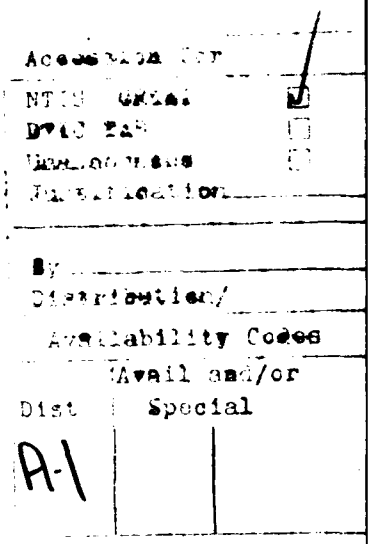

FEBRUARY 1992

U.S. ARMY RESEARCH OFFICE

PROPOSAL NUMBER: 28997-PH
RESEARCH AGREEMENT NO: DAAL03-91-G-0297

DEPARTMENT OF PHYSICS, RUTGERS UNIVERSITY

APPROVED FOR PUBLIC RELEASE
DISTRIBUTION UNLIMITED

THE VIEW, OPINIONS, AND/OR FINDINGS CONTAINED IN THIS REPORT ARE THOSE OF THE AUTHOR(S) AND SHOULD NOT BE CONSTRUED AS AN OFFICIAL DEPARTMENT OF THE ARMY POSITION, POLICY, OR DECISION, UNLESS SO DESIGNATED BY OTHER DOCUMENTATION.

List of Appendixes, Illustrations and Tables

Table of Contents

TIME AND SPACE RESOLVED ELECTRON IMPACT EXCITATION RATES IN AN RF GLOW DISCHARGE

FINAL REPORT

A. Statement of Problem Studied:

Research on rf glow discharge plasmas was carried out to better understand the fundamental physics and chemistry of important aspects of plasma deposition and etching. A standard reference system for rf plasma processing research was utilized. Power, voltage and current waveforms were monitored and time and space resolved measurements were made using plasma induced emission (PIE). Nanosecond time resolution for PIE greatly expanded the utility of these plasma diagnostics over previous studies. Measurements were carried out with a prototype rf model discharge, atomic argon, concentrating on the important 4*s* levels 11.5eV above the ground state and the manifold of *p* levels coupled to these states by strong dipole transitions. Extensive analysis and computer modeling was carried out to reproduce the experimental data obtained and to test assumptions often used for this model system. Models of electron excitation "waves" were stringently tested and evaluated. The research concentrated on studying details of excitation waveforms as a function of pressure and rf power. Information on electron energy distribution functions were derived from the experimental results. New experimental techniques to enhance time and space resolution were developed.

B. Summary of Most Important Results:

In the period 1 August through 31 December, 1991, significant advances in the study of electron kinetics in parallel-plate rf glow discharges was made. The major aspect of the investigation was based on the measurement of space- and time-resolved optical emission using time-correlated single photon counting techniques. An argon discharge between two equal-area plane-parallel electrodes, driven symmetrically at 13.6 MHz, was investigated. This system closely approximates the ideal one-dimensional discharge structure typically treated by modelers in the field. After some analysis, experimental results can be compared with simulation predictions of the rate of electron-impact excitation. This is an essential test of the treatment of electron kinetics in rf discharge models. In fact, the measurement of time- and space-resolved emission spectra has been proposed as a standard diagnostic for the GEC Reference Cell as discussed at the 44th Annual GEC, held in Albuquerque, NM in October 1991.

New features of the process of electron heating by sheath oscillation were found.[1] The dependence of the *range* of sheath-heated electrons on *pressure* was explicitly revealed in space- and time-resolved emission data. (see Figures 1 and 2) This information is important for the verification of simulation results and for the interpretation of data acquired by other techniques. Temporal broadening of electron-impact excitation waveforms was also measured, in agreement with simulation predictions.[2] The effect of finite spatial resolution in optical emission spectroscopy (OES) of the parallel-plate discharge was also illustrated. Essentially, the

accuracy of time-dependent emission data is limited by the spatial resolution of the measurement. This problem results from the 3-dimensional nature of the measurement.

It is a non-trivial matter to determine the spatial resolution of a typical imaging system used for OES. Normally, a portion of the discharge is imaged onto the entrance slit of a monochromator. Previous investigators had found the collection efficiency of such a system for arbitrary points within a discharge volume by extensive ray tracing calculations.[4,5] This method was also used in our initial analysis. However, the ray tracing analysis necessary to determine the spatial response function requires a great deal of programming and computer time. We developed an accurate easy to implement alternate method based on the reasonable assumption of a nearly-ideal lens system.[6] In this approximation, the collection efficiency for an arbitrary point can be found by geometrical arguments, with no need for ray tracing. A system of achromats, each operating at infinite conjugate ratio, easily satisfies the basic assumptions. This method reduces the time required for programming and computation by several orders of magnitude. The accuracy of this method was tested by comparison with exact ray tracing and the agreement was excellent. These results should make absolute calibration and spatial deconvolution of emission data a trivial task for researchers in the field. (see details in Appendix 1).

Several advances were also made in the modeling aspect of this project. A closer examination of a collisional-radiative model of excited levels in an argon discharge led to a number of important simplifications which greatly expand the utility of the model. The

model was developed earlier as part of a diagnostic technique for studying the EEDF in a low-pressure discharge in argon. Using absolute densities of the four argon 4s levels, measured by resonant laser absorption, an electron temperature and density consistent with the model rate balance equations can be found (a Maxwellian EEDF is assumed). A simplified two-level version of this model was found to yield electron temperatures within 10 percent of those found using a more complicated four-level model. This result represents a great simplification in computation and experiment. For the two-level version, the densities of the lowest metastable and resonance levels must be determined. These densities are typically much higher, and therefore, more easily and accurately measured, than the higher lying 4s levels. The main advantage of this method in comparison to the emission line intensity ratio method is that low-energy electrons are also sampled. An extension of the model to account for a two-electron-group EEDF is being considered.

Progress was also been made in developing a "fluid model" code for simulating rf discharges. This type of code is based on the first few moments of the Boltzmann equation for electrons and ions. Our code takes into full consideration the momentum conservation for electrons and ions. The solution is implemented by linearizing the moment equations and adopting a simple implicit method of discretization. Preliminary tests were run on local computers to investigate the stability of the algorithm and to identify possible areas of improvement. After further optimization, the code should be transferred to the facilities at the National Center for Supercomputing Applications (NCSA) at the University of Illinois.

The code will be a powerful asset in guiding experiments and interpreting large amounts of experimental data.

Bibliography

1. M. Colgan, N. Kwon, Y. Li and D.E. Murnick, *Phys. Rev.* Letters **66**, 1858 (1991)
2. D. B. Graves, *J. Appl. Phys.* **62**, 88 (1987)
3. M. Meyyappan, *J. Appl. Phys.* **69**, 8047 (1991)
4. P.B. Farnsworth, B.W. Smith, and N. Omenetto, *Spectrochim.* Acta. **45B**, 1151 (1990)
5. F. Tochikubo and T. Makabe, Meas. Sci. Technol. **2**, 1133 (1991)

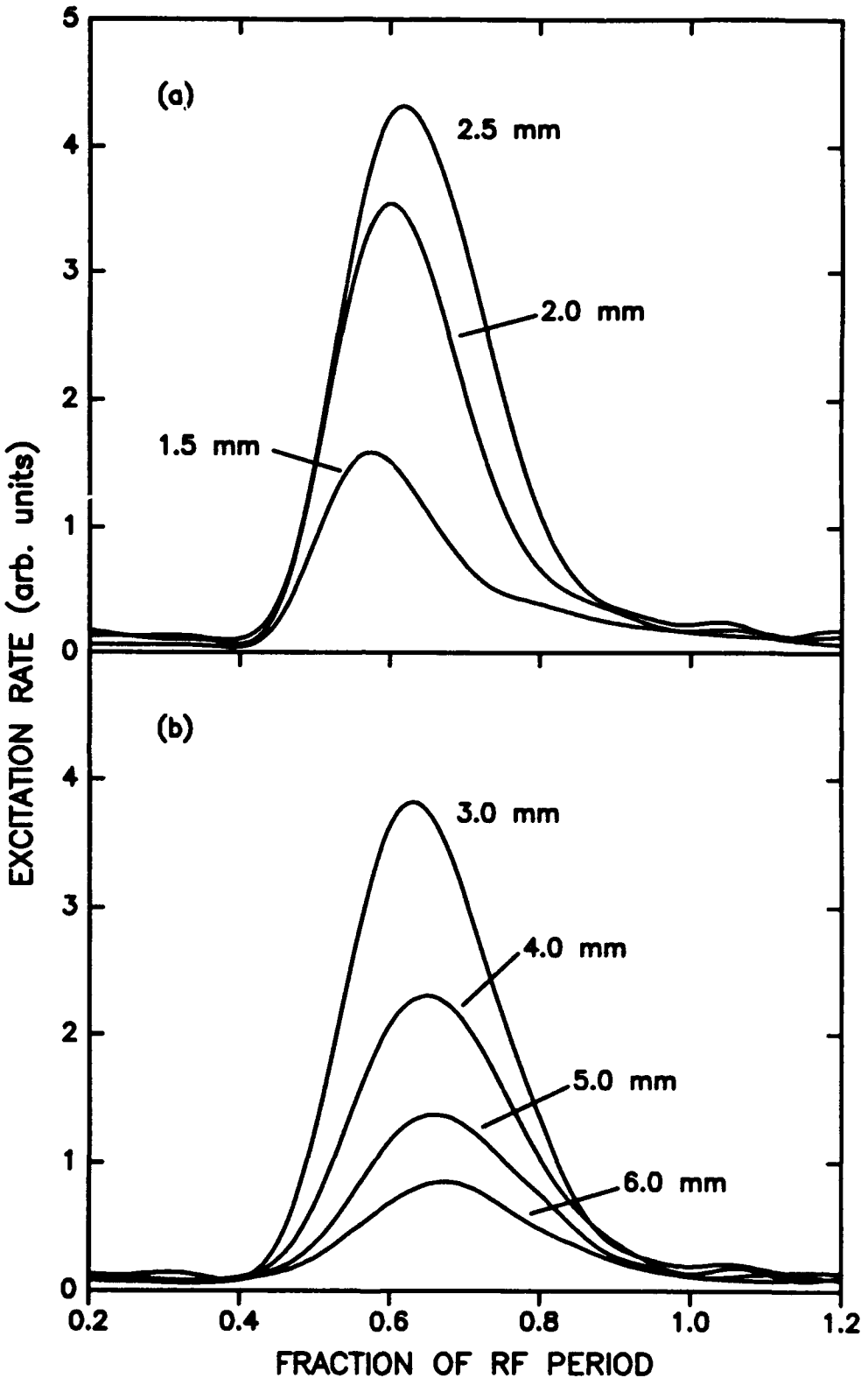

Figure 1. Electron Impact Excitation Waveforms at 1.0 torr argon pressure.

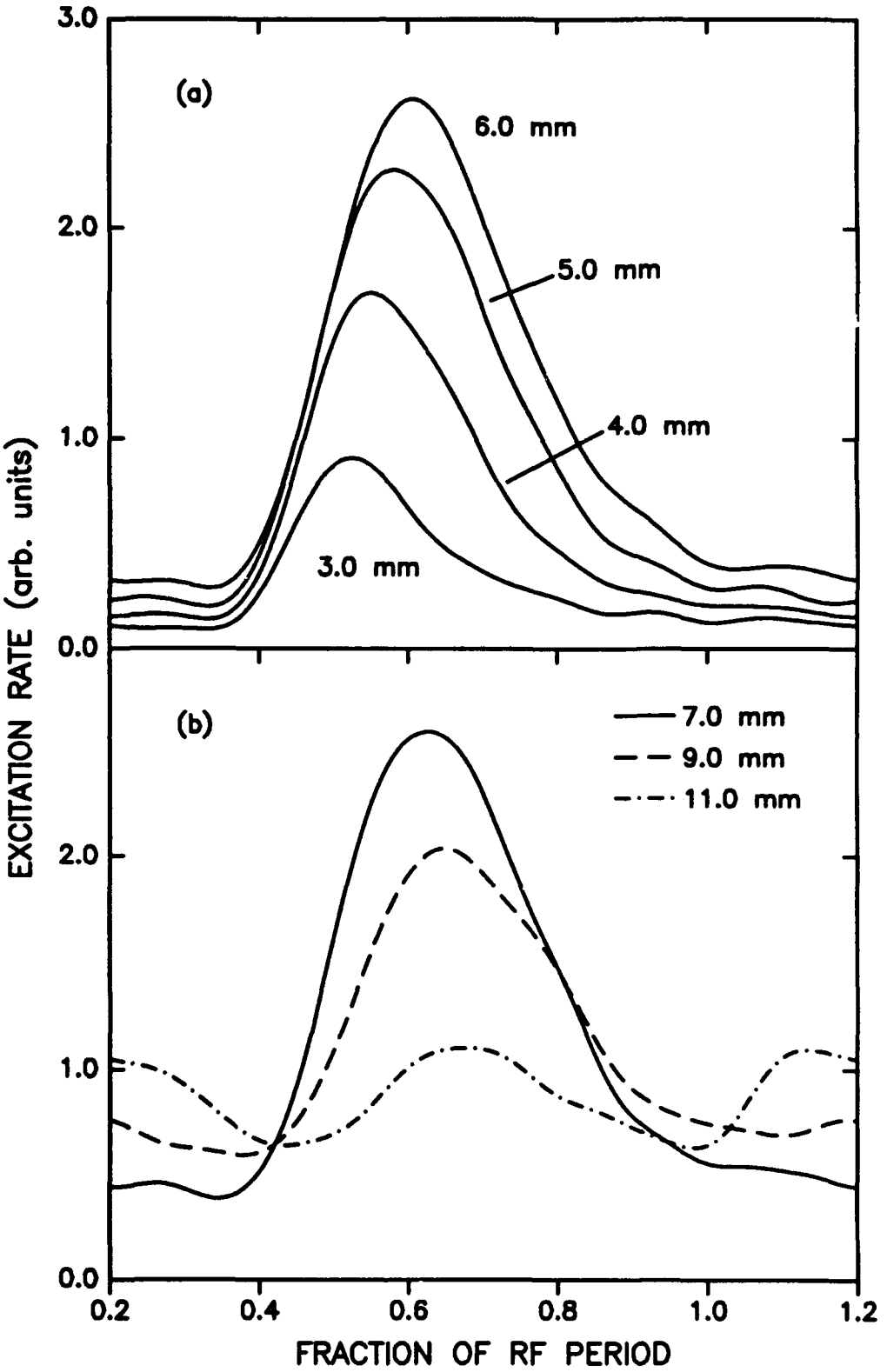

Figure 2. Electron Impact Excitation Waveforms at 0.2 torr Argon Pressure

C. List of All Publications and Technical Reports:

1. Kinetic Processes in Radio Frequency Glow Discharges in Argon, by Michael J. Colgan (Ph.D. thesis Rutgers University, September 1991)
2. Fast Calculation of Collection Efficiency for Optical Emission Spectroscopy of Extended Sources by Michael J. Colgan. Submitted to Review of Scientific Instruments (1992)

D. List of all Participating Scientific Personnel:

Michael J. Colgan, Ph.D. granted October 1991

Xiong He, Post Doctoral Associate

Daniel E. Murnick, PI

Yuan Li, Co-PI

Manuscript submitted to Review of Scientific Instruments

FAST CALCULATION OF COLLECTION EFFICIENCY FOR OPTICAL EMISSION SPECTROSCOPY OF EXTENDED SOURCES

M. J. Colgan

Department of Physics, Rutgers University, Newark, New Jersey 07102

Abstract

A simple method for estimating the collection efficiency of a nearly-ideal optical system is described. Calculation of spatial response functions for the analysis of optical emission data is emphasized. The simple geometric algorithm presented is several orders of magnitude faster than algorithms based on ray tracing. The method is applied to the case of a radially-uniform cylindrical source between parallel plates and the results are in excellent agreement with ray tracing calculations.

FAST CALCULATION OF COLLECTION EFFICIENCY FOR OPTICAL EMISSION SPECTROSCOPY OF EXTENDED SOURCES

M. J. Colgan

Department of Physics, Rutgers University, Newark, New Jersey 07102

I. INTRODUCTION

Optical emission spectroscopy (OES) is a standard technique for detecting atoms and molecules in various excitation sources including glow discharges, plasmas, flames, arcs, etc. In many cases, the excitation source produces an extended source of emission with definite spatial structure. In order to resolve this structure, the spatial response of the measurement system must be determined so that position-dependent emission data can be deconvoluted.

A typical system used for OES consists of imaging optics which collect light from a source and focus the light at the entrance slit of a monochromator. A photomultiplier then detects the light transmitted through the monochromator. The instrument function which describes this system is the product of the efficiency of the detector (monochromator plus photomultiplier) and the collection efficiency of the optics (including the entrance slit of the monochromator). If the entire instrument function is known, position-dependent emission data can be deconvoluted *and* placed on an absolute scale. The detector efficiency can be determined using standard calibration lamps. The collection efficiency of the optical system, however, can be strongly dependent on the coordinates of the point of emission. Accurate calculations of collection efficiency[1,2] are generally based on ray tracing algorithms. While ray tracing is applicable to a wide range of system configurations, the time requirements for computer programming and computation are extensive. An alternative to ray tracing is proposed in this paper which is simple to implement and reduces time

requirements by several orders of magnitude. The case of a parallel-plate discharge is considered as an illustration of the utility of these calculations. The results are also compared with ray tracing calculations as a test of accuracy.

II. METHOD

The optical system under consideration is shown in Fig. 1. The lens system is arbitrary at this point. The y axis coincides with the optical axis and the x axis is parallel to the monochromator entrance slit. The quantity to be determined is the collection efficiency ϵ of this system for an arbitrary point (x, y, z) in the source volume. The source is assumed to be optically thin and losses due to optical elements will be neglected. Isotropic radiation is also assumed. Adopting the ray formalism for now, the rays which are accepted by the entrance slit will form a pattern as they intersect a plane which is tangent to the vertex of the leftmost lens surface at $y = L$ (a convex surface is assumed for convenience). In most cases, the ratio of L to the effective aperture diameter D of the leftmost lens is greater than about 3. For these conditions, the solid angle Ω of light collection from the point (x, y, z) is very nearly equal to the area A defined by the pattern of accepted rays at $y = L$ divided by $(L - y)^2$. The collection efficiency is then given by

$$\varepsilon(x, y, z) = \frac{\Omega}{4\pi} = \frac{A}{4\pi(L - y)^2}. \tag{1}$$

If the lens system is ideal, *i. e.*, free of aberrations, the pattern of accepted rays at $y = L$ can be found very simply. The optical conjugate of the entrance slit is an accurate, possibly magnified, two-dimensional image of the slit in the x-z plane, hereafter referred to as the focal plane. For source points in the focal plane and within the confines of the slit image, the pattern of accepted rays fills the aperture of the leftmost lens. For source points in the focal plane but external to the slit image, no rays are accepted. With these assumptions, the pattern of accepted rays from source points which do not lie in the focal

plane can be easily determined since the line defined by the *initial* path of an accepted ray must pass through the *image* of the slit. The rectangle defined by projecting those rays which connect a source point (x, y, z) with the corners of the slit image onto the plane at $y = L$ limits the paths of rays which might be accepted. The intersection of this rectangle with the lens aperture gives the pattern of accepted rays. The problem has effectively been reduced to simple geometry. The parameters needed for solution are the dimensions and location of the slit image and the diameter of the effective aperture of the leftmost lens.[3] This method of determining collection efficiency will be referred to as the *projection* method, in contrast to the *ray tracing* method.

This ideal imaging system cannot be realized practically. However, the assumptions can be nearly satisfied by a system of two computer-optimized achromats. Given the typical dimensions of a spectrometer entrance slit, minimal spherical aberration is the most important feature of a nearly-ideal lens system. In general, one of the optimization criteria for a computer-optimized achromat is that spherical aberration is reduced to the point where diffraction-limited focusing of parallel light is achieved. In this case, the distance L can be identified as the "back focal length" of the leftmost lens, and is slightly shorter than the focal length f. Note that most achromats are asymmetric elements and proper orientation should be observed.

This degree of restriction on a lens system may not be acceptable in some situations. In particular,[1] cemented doublets are generally not useful for wavelengths below about 400 nm. However, air-spaced achromats with extended ultraviolet transmission ranges are available.

In Fig. 2, a comparison of the patterns of accepted rays found by the ray tracing and projection methods is shown for the source point $(0.48, 0.5, 0.02)$ with coordinates given in units of cm. For this example, the lenses are identical $f = 25$ cm achromats separated by 1.0 cm along the optical axis and operating at an f/number of 5. (The f/number of a lens

is defined as the ratio of focal length to aperture diameter.) The slit and its image both measure 100 μm by 1.0 cm. Standard algorithms[4] were used for ray tracing. The effects of aberrations are apparent in Fig. 2, although the areas enclosed by the two patterns differ by only 4 percent.

The agreement between the ray tracing and projection methods is generally very good, with errors becoming significant only for source points very near the surface of the contributing volume of the discharge. The collection efficiency for these points is very small, however, and is difficult to calculate even by ray tracing. When the collection efficiency of an optical system is calculated by ray tracing, the rays typically pass through fixed grid points on a lens aperture or some other plane. The accuracy for source points with small contributions is limited by the spacing of this grid. This discrete nature of the ray tracing method was pointed out in Ref. 1. The only way to improve the accuracy for these source points is to decrease the grid spacing and trace a larger number of rays. However, as noted in Ref. 1, tracing even a modest number of rays (8000) may require several minutes of computer time per source point. The error due to tracing a finite number of rays can easily be larger than the error due to the neglect of aberrations in the projection method. In many applications, however, these sources of error can be neglected based on the low collection efficiency of the source points in question.

III. APPLICATION TO A PARALLEL-PLATE SOURCE

As an example of the utility of these calculations, the case of a radially-uniform, cylindrical parallel-plate discharge will be considered. For this geometry, there are significant variations in emission intensity along the discharge axis for both DC and AC excitation.[5] Spatially-resolved emission spectroscopy can determine excitation, ionization, and dissociation rates yielding important information regarding local kinetic processes and discharge

sustaining mechanisms.

The discharge axis is assumed to coincide with the z axis in Fig. 1. The height of the optical axis above the lower electrode will be denoted by z_0. The measured photon count rate (single photon counting is assumed for the detection mode) is then $\alpha(z_0)$ and the emission rate per unit volume is $\Phi(x, y, z + z_0)$. The relation between these two quantities can be written as

$$\alpha(z_0) = \varepsilon_0 \sum_{x,y,z} \varepsilon(x, y, z, z_0)\Phi(x, y, z + z_0)\Delta x \Delta y \Delta z \tag{2}$$

where ε_0 is the efficiency of the detector (including the monochromator) and $\varepsilon(x, y, z, z_0)$ is the collection efficiency for the source point $(x, y, z + z_0)$. The sums over x, y, and z represent an integration over the entire discharge volume. The influence of a nearby electrode on a measurement has been included by making ε a function of z_0 as well as x, y and z. If radial variations are neglected, eq. (2) can be simplified to

$$\alpha(z_0) = \varepsilon_0 \sum_{z} R(z, z_0)\Phi(z + z_0)\Delta z \tag{3}$$

where

$$R(z, z_0) = \sum_{x,y} \varepsilon(x, y, z, z_0)\Delta x \Delta z \tag{4}$$

is the axial response function. Far from either electrode, $R(z, z_0)$ is independent of z_0 and the notation $R(z, \infty)$ will generally be used unless the effect of a nearby electrode is being investigated. As discussed earlier, equation (3) represents the convolution of the actual emission distribution and the instrument function $\varepsilon_0 R(z, z_0)$.

This analysis would also be applicable to the case of time-dependent emission, as in a radio frequency parallel-plate discharge.[2,6] In that case, α and Φ would be functions of time as well as position in equations (2) and (3). The distortion caused by the measurement system also effects the *time*-dependence of emission data measured in these discharges.

In Ref. 6, this effect was simply illustrated by reducing the f/number of the optics. The temporal widths of electron-impact excitation waveforms which were derived from the emission data revealed a rather strong dependence on the f/number of the collection optics. The treatment considered here, which is similar to that presented in Ref. 2, is a more efficient solution to this problem.

In Fig. 3, $R(z, \infty)$ is shown as calculated by ray tracing and by the projection method described in the previous section. The agreement here is excellent. The elements Δx and Δy were chosen so that the variation in ε was small across either distance. In this case, Δx was set to 0.02 cm and Δy varied from 0.02 cm near the discharge axis to 0.1 cm near the edges of the discharge. $R(z, \infty)$ was calculated for a limited number of z values by the ray tracing method because of the extensive computer time involved. For this example, the discharge was 7.62 cm in diameter ($x^2 + y^2 < 14.2$ cm^2 in eq. (4)) and the slit measured 100 μm by 1.0 cm. The lenses were both 25 cm focal length, $f/5$ achromats (unity magnification) and were separated by 1.0 cm along the optical axis.

A rigorous series of tests was performed to determine the limitations of the projection method. Accuracy was not affected by changes in the focal length or f/number of the lenses, by magnification other than unity (using two lenses with different focal lengths), or by changes in the diameter of the discharge. Among the more critical tests was the reduction of the 100 μm width of the entrance slit. The agreement with ray tracing calculations was retained down to a width of 20 μm. For a 10 μm wide slit, a difference of 10 percent was observed at the peak of the response function ($z = 0$). However, the validity of ray tracing for such a narrow slit is questionable when diffraction is considered. The diameter of the Airy disk[4] for a lens is $2.44\,\lambda\, f/D$ or about 6 μm for an $f/5$ lens and incident light of wavelength $\lambda = 500$ nm. The diffraction-limited minimum spot size is thus nearly equal to one of the slit dimensions. The projection method therefore has roughly the same limitations as ray tracing in terms of a minimum slit width. Slit widths up to 400 μm and

slit lengths between 0.2 and 2.0 cm were also tested, demonstrating agreement between the two methods for all cases.

Optical systems are usually separated from a source by a window which should be considered as an optical element. The primary effect of a window is a displacement of the image along the optical axis. This displacement will be very small relative to the dimensions of an extended source for reasonable glass thickness. Quartz plates up to 1.2 cm thick were added between the discharge and the lens system considered above. $R(z, \infty)$ was then recalculated by the ray tracing method verifying that the plates had no detectable effect, even when the slit width was reduced to 20 μm.

Another parameter which might affect the accuracy of the projection method is the separation between the two lenses. In this case, ray tracing showed a negligible change in $R(z, \infty)$ for a separation of 10 cm and a 5 percent reduction in amplitude for a separation of 20 cm. This small change is probably due to vignetting and residual abberation. Serious errors might be expected for very large lens separations.

The effect of a nearby electrode can be investigated with a minor modification of the projection algorithm. Reflections from the electrode will be neglected here as well as the curvature of the electrode edge facing the lens system. The pattern of accepted rays is adjusted so that rays which would strike the electrode are eliminated and, of course, there is no emission from points below the electrode surface. In Fig. 4, the axial response function $R(z, z_0)$ is shown for $z_0 = \infty$ and for $z_0 = 0$ (optical axis in the plane of the electrode surface). For positive z, the ratio $R(z, 0)/R(z, \infty)$ is about 0.5. This is because the light emitted from nearly all source points with negative y is blocked by the electrode when $z_0 = 0$. As z_0 increases, the shape of $R(z, z_0)$ becomes rather complex before assuming the shape of $R(z, \infty)$. The effect of any perfectly absorbing obstruction between the source and the lens system can be found in a similar way.

A flat, smooth reflecting surface can also be handled rather simply by considering the

images of the source points. In the case of a nearby plate electrode the image of the source point $(x, y, z + z_0)$ is $(x, y, -(z + z_0))$. The collection efficiency for the image point can be calculated as if no electrode was present and then multiplied by the reflectivity of the electrode surface. The resulting value should then be added to the collection efficiency for the real source point $(x, y, z + z_0)$.

Useful results can be obtained with the projection method on very short time scales. While this feature is generally appealing, it could be a real advantage in situations where the system parameters are changed during the course of an investigation. For example, the spectrometer slit width might be reduced to improve the wavelength resolution. As noted earlier, a moderate-resolution ray tracing determination of collection efficiency for one source point might require several minutes of computation on a personal computer.[1] In contrast, the results shown in Fig. 3 (solid line) were generated in five minutes using the projection method on a personal computer. For that curve, collection efficiencies for more than 10^5 source points were calculated.

IV. SUMMARY

A simple method for estimating collection efficiency and calculating spatial response functions for optical emission spectroscopy of extended sources has been presented. Results for the cylindrical parallel-plate discharge geometry were compared with ray tracing calculations showing excellent agreement for a wide range of system parameters. The conditions for which the method is applicable place some restrictions on the lens system which may be used for imaging. The fundamental restriction is that spherical aberration must be negligible. This condition is easily satisfied by a system of two optimized achromats, each operating at infinite conjugate ratio. Due to the simplicity and speed of the algorithm, the effects of parameter changes in the optical system can be rapidly evaluated.

The response functions calculated in this manner can be used to remove the distortion of position-dependent emission data caused by a measuring system, and to determine an absolute scale for emission rates.

ACKNOWLEDGEMENTS

Helpful discussions with D. E. Murnick and Y. Li are gratefully acknowledged. This work was supported in part by the U.S. Army Research Office.

REFERENCES

[1]P. B. Farnsworth, B. W. Smith, and N. Omenetto, Spectrochim. Acta. **45B**, 1151 (1990).

[2]F. Tochikubo and T. Makabe, Meas. Sci. Technol. **2**, 1133 (1991).

[3]While the effects of any additional stops (limiting apertures) can be taken into account by ray tracing, this is not the case for the projection method described here. The aperture for the lens closest to the source should function as the aperture stop for *all* object points in the source volume.

[4]C. S. Williams and O. A. Becklund, *Optics: A Short Course for Engineers & Scientists* (Krieger, Malabar, Fla., 1984).

[5]B. N. Chapman, *Glow Discharge Processes* (Wiley, New York, 1980).

[6]M. J. Colgan, N. Kwon, Y. Li, and D. E. Murnick, Phys. Rev. Lett. **66**, 1858 (1991).

FIGURE CAPTIONS

FIG. 1. Schematic of the optical system.

FIG. 2. Sample pattern of accepted rays at $y = L$. The pattern of accepted rays determined by the projection method (dashed line) is in good agreement with the pattern found by ray tracing (solid line). The areas enclosed by such patterns are used in the calculation of collection efficiency and differ by only 4 percent. These patterns were generated for the source point $(0.48, 0.5, 0.02)$ (see Fig. 1). For comparison, the pattern of accepted rays for a point with maximum collection efficiency, *i. e.*, the point $(0, 0, 0)$, would fill the area enclosed by $x^2 + z^2 = 2.5^2$.

FIG. 3. Axial response function for a radially-uniform cylindrical source. The system parameters are given in the text. Nearly identical results are found by the projection and ray tracing methods. Good agreement is maintained over a wide range of system parameters.

Fig. 4. Effect of a perfectly absorbing planar electrode on the axial response function. When the optical axis is at the surface of the electrode ($z_0 = 0$) there is no source for $z < 0$ and $R(z, 0) = 0$. For $z > 0$, nearly all the emission from source points with $y < 0$ is blocked by the electrode and $R(z, 0)/R(z, \infty) \simeq 1/2$. Smooth, reflecting planar surfaces can also be treated simply using the method described in this paper.

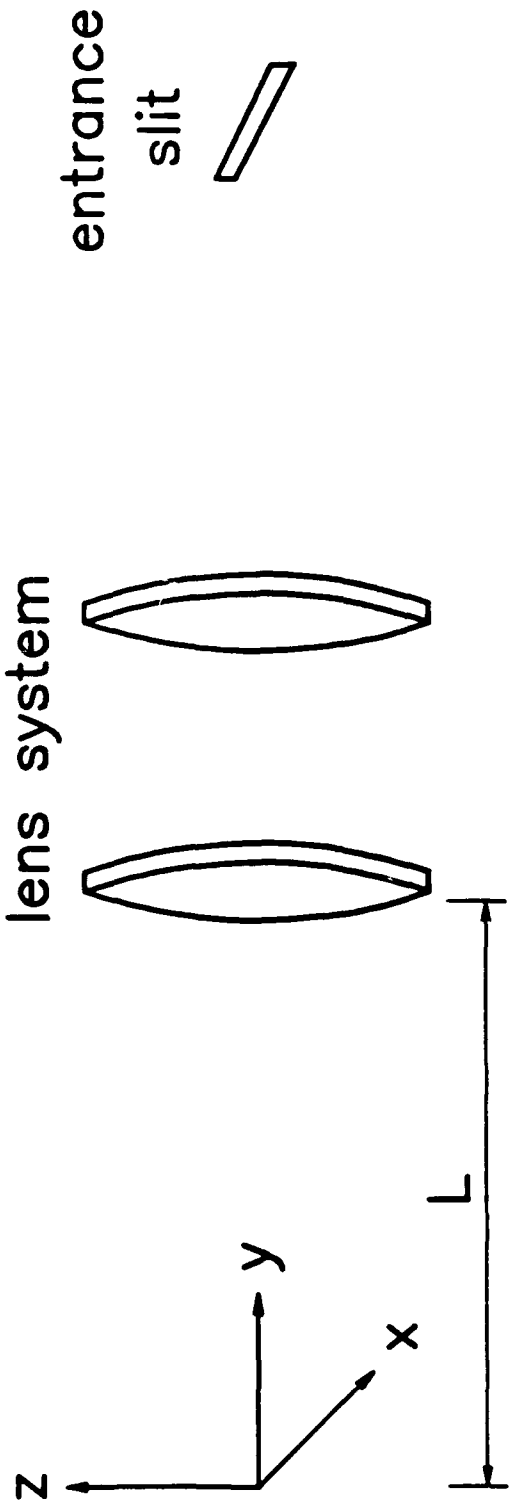

FIG. 1.

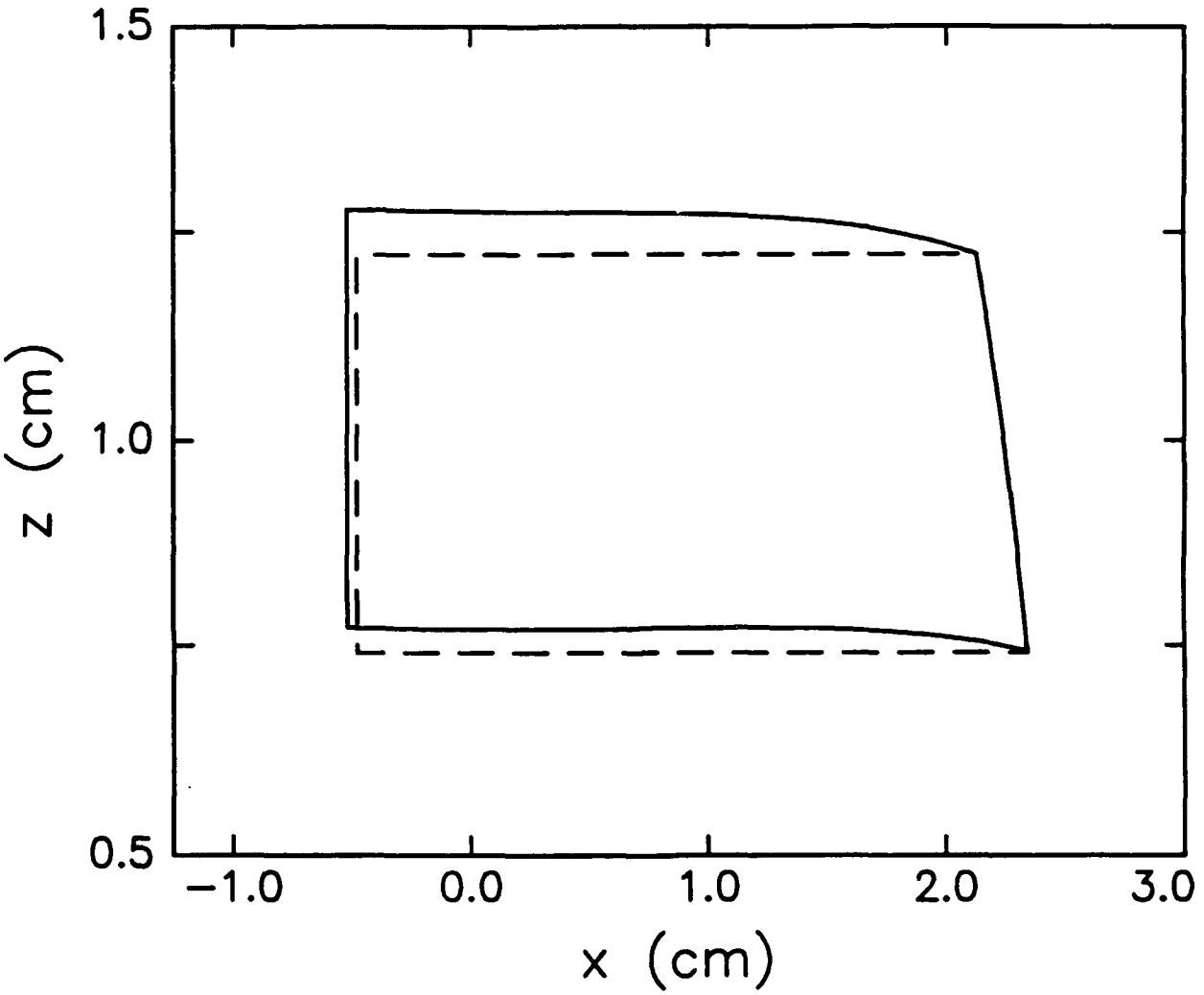

FIG. 2.

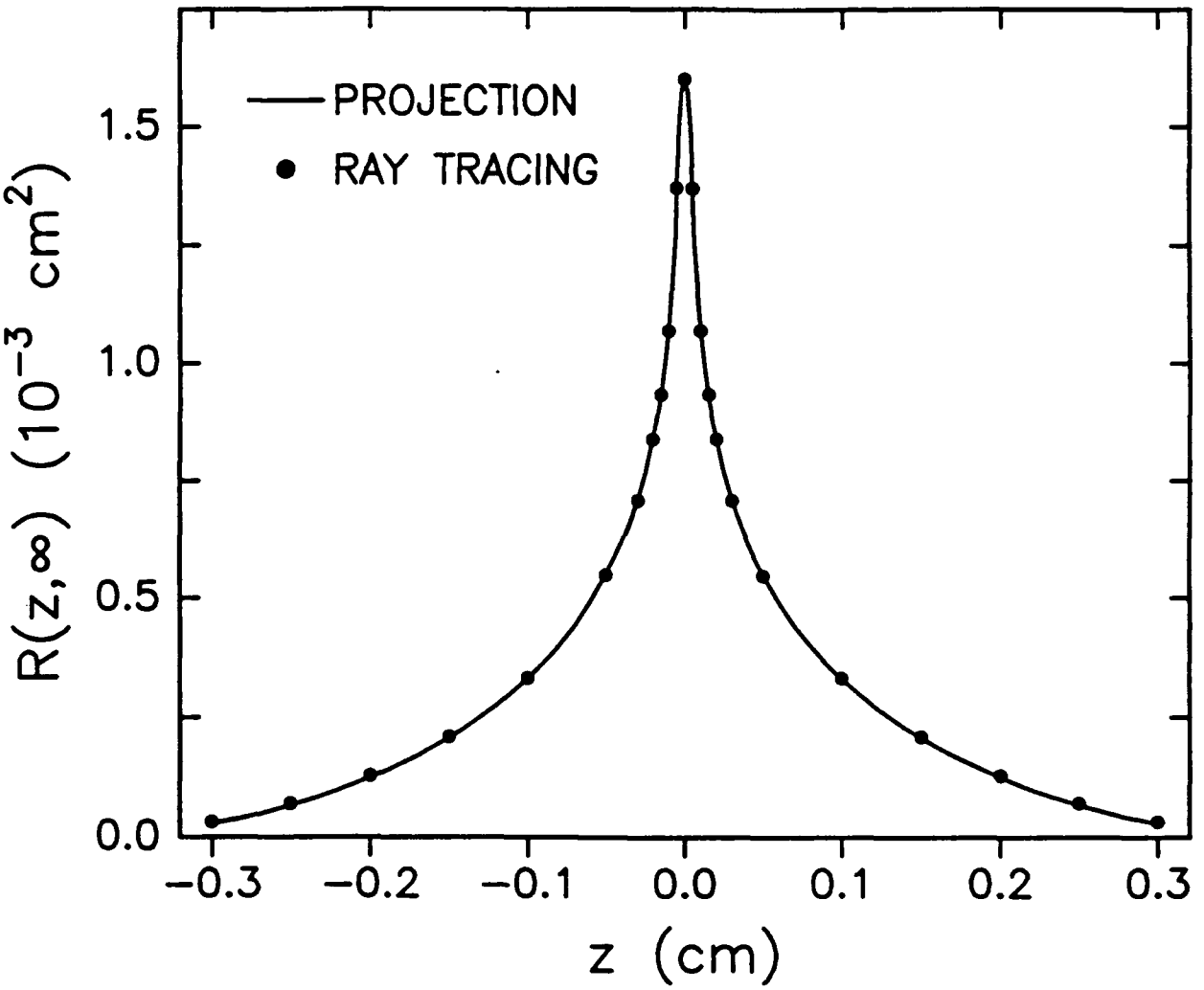
PROJECTION
RAY TRACING
1.5
1.0
0.5
0.0
R(z,∞) (10⁻³ cm²)
−0.3
−0.2
−0.1
0.0
0.1
0.2
0.3
z (cm)

FIG. 3.

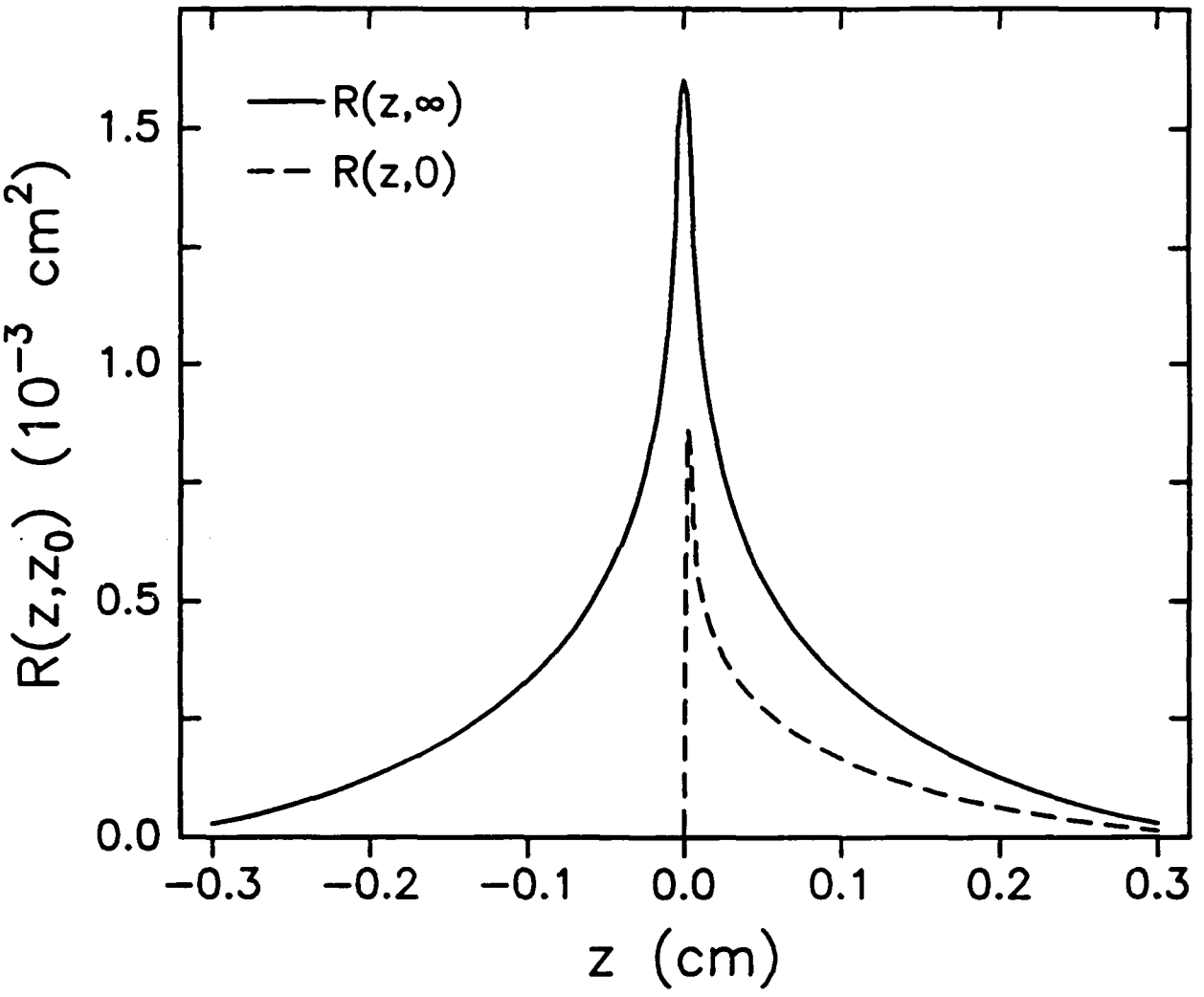

FIG. 4.